Optics Communications 426 (2018) 341–347

Contents lists available at ScienceDirect

Optics Communications

journal homepage: www.elsevier.com/locate/optcom

Sensing of toxic chemicals using polarized photonic crystal fiber in the terahertz regime

Md. Saiful Islam [a,*], Jakeya Sultana [a], Alex Dinovitser [a], Kawsar Ahmed [b], Brian W.-H. Ng [a], Derek Abbott [a]

[a] National T-Ray Facility, School of Electrical & Electronic Engineering, The University of Adelaide, SA 5005, Australia
[b] Department of Information & Communication Technology, Mawlana Bhashani Science & Technology University, Tangail, 1902, Bangladesh

ARTICLE INFO

Keywords:
Terahertz sensor
Photonic crystal fiber
Birefringence
Waveguide
Cyanide

ABSTRACT

Cyanide (CN) is a highly toxic chemical agent that is considered extremely harmful to humans. Considering the level of toxicity and harmfulness to human it is important to have an efficient and flexible detection method of CN. Based on this requirement, we propose a photonic crystal fiber (PCF) based terahertz sensor for the detection of CN. In a Zeonex substrate we use symmetrical and asymmetrical core structures inside a suspension type cladding. The possible sensor architecture and methodology of sensing is also addressed. The fabrication of the proposed sensors is feasible employing existing fabrication technology.

1. Introduction

Cyanide is a chemical compound that consists of a triple bonded carbon atom to a nitrogen atom ($C \equiv N$). It is colorless, volatile, poisonous and fast acting chemical that depending on the level of exposure it can result in mortality within a minute [1]. Cyanide is used as an essential reagent for different industries such as mining and petroleum, electroplating, plastics and steel manufacturing, tanning, silver and gold extraction, automobile manufacture, synthetic fiber production and metallurgy [2]. However, the exposure of cyanide to humans is harmful and the above mentioned industries are mainly responsible for it because the possibility of CN exposure increases during heavy use and transportation. Biological sources such as fungi, bacteria and algae produce CN as part of their nitrogen (N) metabolic pathways. Dietary foodstuffs including cassava, lima beans, linseed, sweet potatoes, kernels of fruits, sorghum and bamboo shoots contain moderate to high levels of cyanogenic glycosides and these vegetables are considered to be main sources of cyanide ingestion to humans and animals. Moreover, tobacco smoke is also a common source of cyanide ingestion that transfers to blood cells [3]. Cyanide inhibits the normal respiratory function of tissue and cells because it irreversibly binds the iron atom to the hemoglobin that inhibits the hemoglobin from transporting oxygen (O_2) to the respiratory organs. Therefore, it is of utmost importance to discover a suitable method for cyanide detection.

Thus far, several cyanide detection modes such as chromatographic [4], electrometric [5], titrimetric [6], potentiometric [7] and voltammetric [8] techniques have been developed earlier but have drawbacks due to a long analysis time, complex methodology and the need for a skilled user. Therefore, to eliminate the problems faced by the mentioned methods colorimetric strategies have been proposed [9]. The advantage of a colorimetric method is that it is cost effective and possible to detect CN with the naked-eye. However, such a method requires the use of sophisticated instruments with high detection limit. Later, in order to detect low concentration levels a fluorescence technique proved to be a more-powerful optical technique due to its simplicity in operation and rapid implementation.

Photonic crystal fiber is a promising technology nowadays for sensing due to its powerful light–matter interaction property. In a PCF the light guiding property such as material absorption loss, amount of core power, birefringence, confinement loss and dispersion can be modified by tuning its geometrical parameters such as core diameter, pitch distance, shape of air holes, air hole size that is not possible by using conventional optical fiber. Moreover in a PCF, instead of using air inside the air holes we can use different analytes (gas/chemicals/biological molecules) to use it in a sensing application [10]. In 2006, Cordeiro et al. [11] investigated a PCF based sensor using different analytes in the core air holes. In recent years, for chemical sensing a number of PCF designs [12–15] are reported in the optical wavelength. Moreover, considering the impact of employing terahertz we proposed a PCF based chemical sensor using a kagome structure in the cladding and a rectangular air hole structure in the core. We obtained a high chemical sensitivity with low loss [16] however the kagome structure is difficult

* Corresponding author.
E-mail address: mdsaiful.islam@adelaide.edu.au (M.S. Islam).

https://doi.org/10.1016/j.optcom.2018.05.030
Received 14 February 2018; Received in revised form 15 April 2018; Accepted 9 May 2018
Available online 22 June 2018

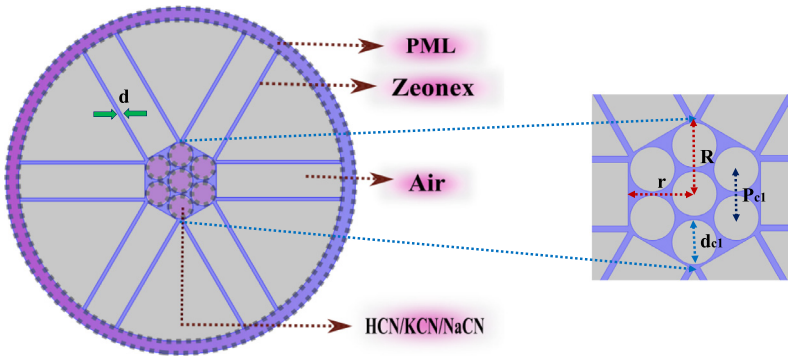

Fig. 1. Schematic of the proposed sensor type-I.

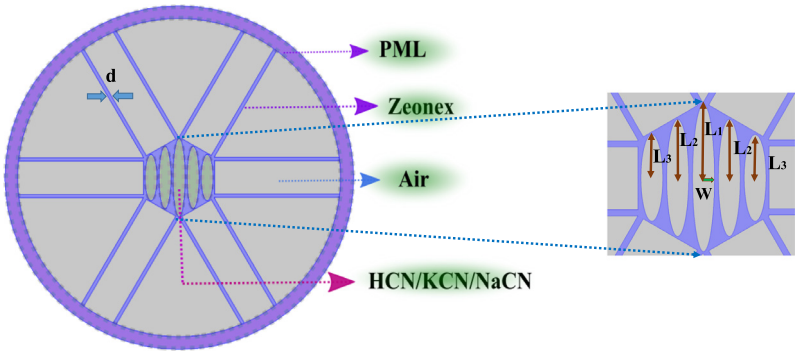

Fig. 2. Schematic of the proposed sensor type-II.

to fabricate. Thus, considering the complexity of fabrication we provided a solution and designed a suspension type cladding that reduces the fabrication complexity than the kagome structure [17] as it does not contain any over-lapped rectangular parallel struts in the cladding region. Another advantage of the proposed PCFs over the conventional kagome PCF is that it is cost effective as it requires less material in the cladding during fabrication.

In this manuscript, utilizing the benefits of PCF we propose two PCF based sensors for toxic cyanide detection in the terahertz band. Instead of using a kagome structure we propose a more fabrication-ready suspension type cladding that consists of few rectangular struts. In the core of the PCF we use one symmetrical and one asymmetrical structure and characterize their sensing performances. Moreover, considering the fabrication tolerance we vary the core air hole size to determine how sensing performance varies with that. Besides sensitivity we also characterize other important optical properties such as effective material loss, confinement loss, bending loss and birefringence of both the proposed sensors.

2. Modeling of the proposed terahertz sensor

In PCF type-I, inside a suspension type cladding we use a hexagonal structure having circular shaped air holes. This is the extension of our previously published research work [17]. Note that, considering the fabrication tolerance we choose the values of core air hole diameter (d_c) and pitch distance (p_{c1}) and ensures sufficient distance between the air holes. See Figs. 1 and 2.

In PCF type-II, we used array of elliptical shaped air holes in a suspension type cladding. The reason for elliptical air holes is to introduce birefringence that is necessary for improving the sensing performance of a terahertz sensor [16]. In PCF type-II, the major axis and minor axis length of elliptical air holes are defined as L, L_1, L_2 and w respectively.

In both PCFs, the strut thickness (d) is kept fixed at 6 μm. Considering the fabrication tolerance, we could reduce the thickness down to 2 μm but we kept it at 6 μm so that the scattering effect due of a suspension type cladding can be reduced. The commonly used polymer material Zeonex (COP) is used as the background material for both PCFs as Zeonex has a number of superior characteristics suitable for terahertz compared to other polymer materials [18].

Note that, the practical realization of proposed PCFs are straightforward as there are existing technologies to fabricate these. Note that, the circular shaped air holes can easily be achieved using the capillary stacking technique whereas the elliptical and rectangular shaped air holes are obtainable by the extrusion and 3D printing techniques [19,20].

3. Analysis of numerical results and discussion

The electric field distribution of both the PCFs is shown through Figs. 3 and 4. For PCF type-I only one polarization mode is considered because of the circular shaped air hole in the core that will experience negligible birefringence. However, analyzing the direction of E-field in Fig. 3 it can be seen that fields are propagating only in one direction and thus it is considerable that PCF-I will operate in the single mode condition.

However, in PCF type-II the E-field distribution of both polarization modes is considered as the core is asymmetrical. At 1.8 THz the obtained effective refractive index of HCN for the x and y polarization modes are 1.248 and 1.254 respectively. Thus the simulation result indicate that there can be other modes present in the waveguide however for those modes the E-field will propagate through the cladding and not from the core. Thus when a fundamental Gaussian beam is launched at the center of the PCF only the fundamental modes will be excited and propagate through the core [16,21]. The modified total internal reflection (MTIR) light guiding mechanism works for both the proposed PCF as the core refractive index is larger than the refractive index of cladding.

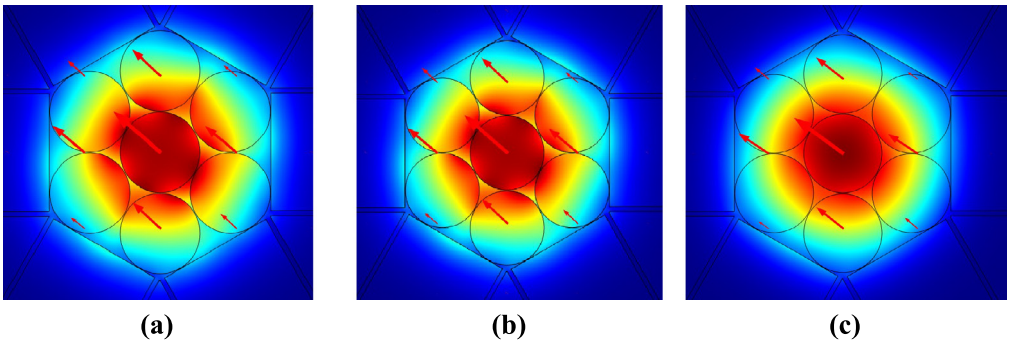

Fig. 3. E-field distribution of sensor type-I for (a) HCN, (b) KCN, and (c) NaCN at $f = 2.0$ THz and $(d_c) = 46.6$ μm.

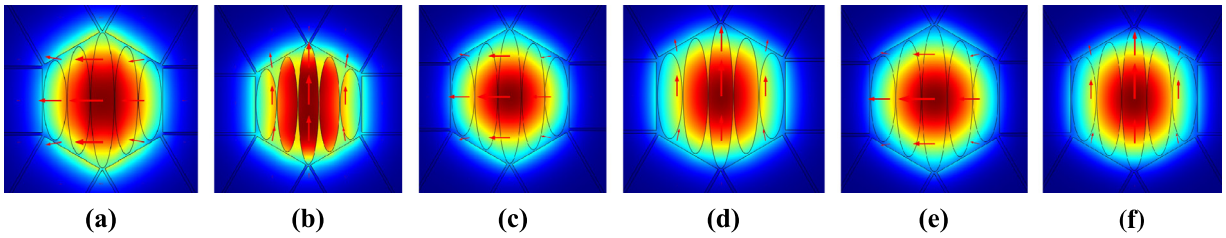

Fig. 4. E-field distribution of sensor type-II for (a) HCN, x-pol, (b) HCN, y-pol, (c) KCN, x-pol, (d) KCN, y-pol, (e) NaCN, x-pol, (f) NaCN, y-pol, at $f = 1.8$ THz and $w = 24.75$ μm.

According to the Beer–Lambert law, the relative sensitivity of a PCF can be obtained. The equation is given by [14],

$$I(f) = I_0(f)\exp[-r\alpha_m l_c] \tag{1}$$

where, $I(f)$ and $I_0(f)$ are the intensities of light with and without the presence of the analyte need to be detected, r represent the relative sensitivity, α_m indicate the absorption coefficient, l_c is the channel length and f is the operating frequency.

The absorbance of the analytes to be detected can be calculated by [14],

$$A = \log\left(\frac{I(f)}{I_0(f)}\right) = -r\alpha_m l_c. \tag{2}$$

The relative sensitivity of the sensor can be calculated by [16],

$$r = \frac{n_r}{n_{\text{eff}}} \times S \tag{3}$$

where, n_r represent the refractive index of the analyte needs to be detected which is 1.26 in case of HCN, 1.41 for KCN and 1.45 in case of NaCN. Note that, liquid form of HCN, KCN and NaCN is considered in both the proposed sensor. Here, n_{eff} denotes the guided mode effective refractive index and S is the proportion of light interaction with the analyte that can be calculated by [16],

$$S = \frac{\int_{\text{sample}} R_e(E_x H_y - E_y H_x)\, dxdy}{\int_{\text{total}} R_e(E_x H_y - E_y H_x)\, dxdy} \times 100 \tag{4}$$

here, E_x, E_y and H_x, H_y are the electric field and magnetic field components of the guided modes respectively.

Figs. 5–7 shows the relative sensitivity of the proposed PCF type-I for HCN, KCN, and NaCN respectively. It can be observed that, relative sensitivity increases with the increase of frequency of up to 2.0 THz and then decreases gradually. The is because, the core power fraction reaches its maximum at 2.0 THz and further increase of frequency causes the reduction of core power fraction. However, at the same time the value of n_{eff} continues to increase that causes reduction of relative sensitivity. Thus, we choose 2.0 THz as optimum operating frequency for PCF type-I.

For PCF-I, by considering the fabrication tolerance we choose optimum $d_{c_1} = 24.75$ μm. However, we observed the sensor characteristics at

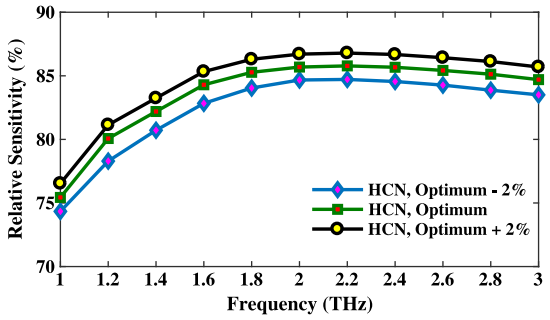

Fig. 5. Relative sensitivity of HCN of PCF-I with respect to frequency at different d_{c_1}.

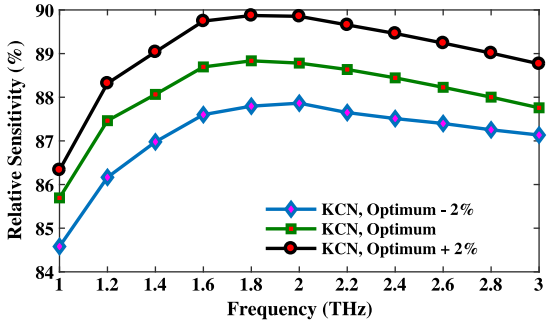

Fig. 6. Relative sensitivity of KCN of PCF-I with respect to frequency at different d_{c_1}.

±2% variation because it is well known that during standard fabrication fluctuation from optimum parameter of a PCF can happen. It can be observed that, 2% increase of d_{c_1} from optimum increases the relative sensitivity because such increment increases the amount of analytes inside the air holes. However, 2% decrease of d_{c_1} also decreases the relative sensitivity as a lower amount of analyte can be filled in a

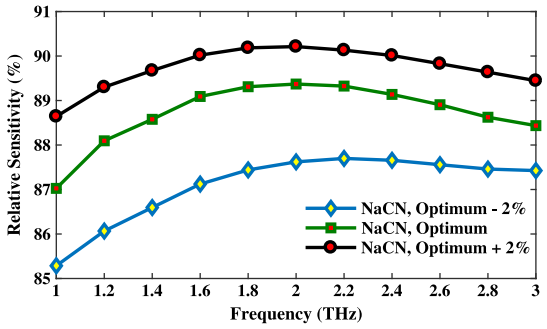

Fig. 7. Relative sensitivity of NaCN of PCF-I with respect to frequency at different d_{c_1}.

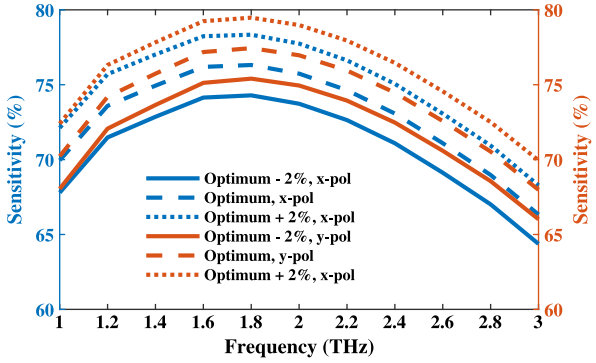

Fig. 8. Relative sensitivity of HCN of PCF-II with respect to frequency at different w, fixed major axis length and orthogonal polarization modes.

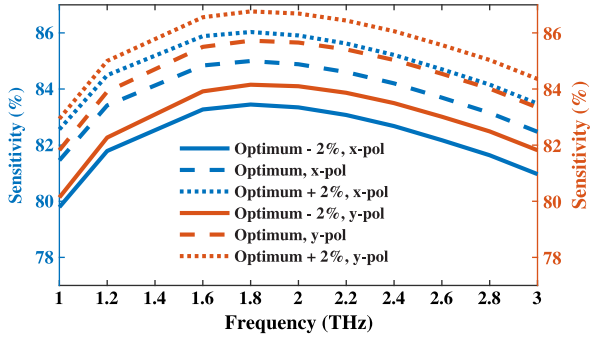

Fig. 9. Relative sensitivity of KCN of PCF-II with respect to frequency at different w, fixed major axis length and orthogonal polarization modes.

smaller d_{c_1}. Therefore, considering all of the above mentioned fact we considered d_{c_1} = 24.75 μm as optimum. Moreover, we can see from Figs. 5–7 that highest relative sensitivity is experiences for NaCN because of its high refractive index than HCN and KCN. Theoretically, it is correct because from Eq. (3) we can see that sensitivity is proportional to the analyte refractive index. Thus, at optimum d_{c_1} and f the relative sensitivity for HCN, KCN and NaCN is 85.8%, 88.8%, and 89.4% respectively.

Now, the relative sensitivity of HCN, KCN and NaCN of PCF-II for both x and y polarization modes are shown through Figs. 8–10. From where it can be seen that relative sensitivity for y-polarization mode is higher than x-polarization mode. The is because core power experiences largely to the y-polarization mode than the x-polarization mode. Therefore, we choose y-polarization mode as optimum for the PCF-II. Figs. 8–10 also indicate that the relative sensitivity for different elliptical minor axis length w is observed. Where, it can be seen that

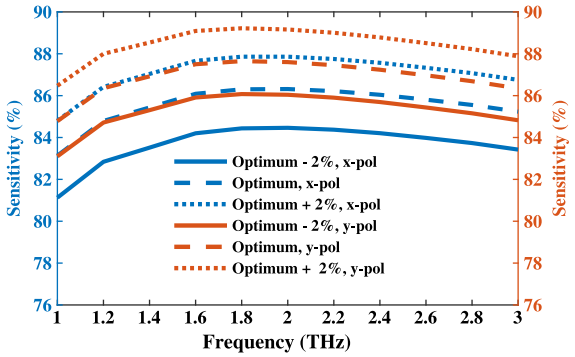

Fig. 10. Relative sensitivity of NaCN of PCF-II with respect to frequency at different w, fixed major axis length and orthogonal polarization modes.

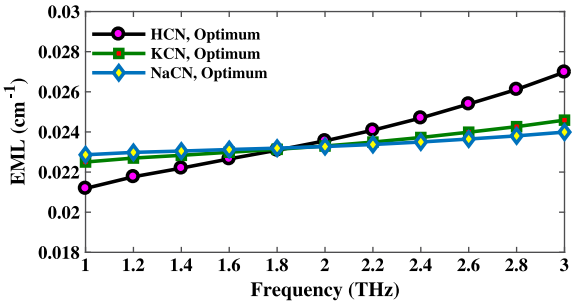

Fig. 11. Effective material loss of PCF-I with respect to frequency at optimum d_{c_1} and d.

sensitivity increases with higher w because of more light interaction with the analytes. It is found that highest relative sensitivity is obtained at 1.8 THz and thus we considered 1.8 THz as optimum. Therefore, at optimum design conditions the relative sensitivity of HCN, KCN and NaCN for PCF-II is 77.5%, 85.7%, and 87.6% respectively.

In terahertz band most of the polymer materials are very much leaky thus experience different types of losses during transmission. Therefore, in designing a terahertz sensor we must consider different types of loss mechanisms that can take place due to the bulk material as well as the waveguide structure. The most important loss mechanisms are effective material loss (EML), confinement loss, and bending loss. The other loss mechanisms are scattering loss and coupling loss. We neglect to calculate the scattering loss as in both the PCF light is strongly confined in the core area and having negligible interaction of light between the core-cladding interface. Moreover, due to high core power fraction the coupling loss is also negligible thus we also neglected to calculate coupling loss. The main loss mechanism known as EML can be calculated by [22],

$$\alpha_{\text{eff}} = \sqrt{\frac{\epsilon_0}{\mu_0}} \left(\frac{\int_{\text{mat}} n_{\text{mat}} |E|^2 \alpha_{\text{mat}} \, dA}{\left| \int_{\text{all}} S_z \, dA \right|} \right) \tag{5}$$

here, ϵ_0 is the permittivity, μ_0 denotes the permeability into free space, n_{mat} and α_{mat} indicates the refractive index and bulk absorption loss of Zeonex respectively, S_z denotes the z-component of Poynting vector in the direction of wave propagation, where, $\mathbf{E}$ is the electric field and $\mathbf{H}^*$ is the complex conjugate of the magnetic field.

Figs. 11 and 12 shows the characteristics of EML of both the PCF with respect to frequency. It can be seen that EML increases with frequency. It can also be observed that the slop of EML increment is high for HCN than KCN and NaCN because HCN have low refractive index than the other two therefore light scattering to the other region from the core is high for HCN. From Figs. 11 and 12 it can be observed that the obtained EML in both the PCFs is very low that is suitable for low loss transmission of terahertz waves for sensing applications.

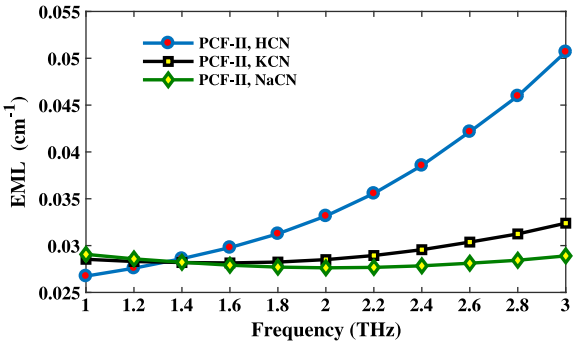

Fig. 12. Effective material loss of PCF-II with respect to frequency at optimum w and d.

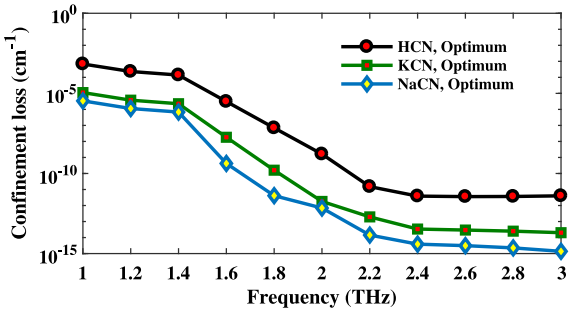

Fig. 13. Confinement loss of PCF-I with respect to frequency at optimum value of d_{c_1} and d.

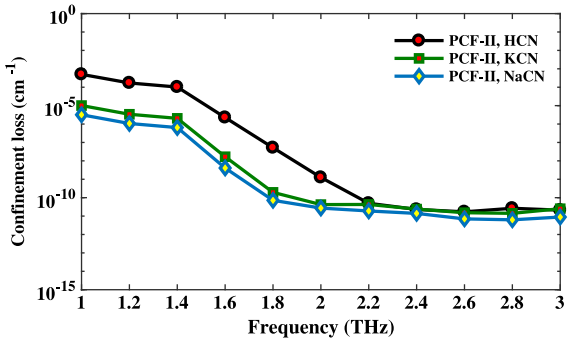

Fig. 14. Confinement loss of PCF-II with respect to frequency at optimum value of w and d.

Another loss mechanism known as confinement loss that indicate the light confining ability of a fiber in the core area is also an important PCF properties to be considered for designing an efficient PCF based sensor. It determines the length of terahertz transmission through the fiber. It can be calculated by the equation [16],

$$L_c = \left(\frac{4\pi f}{c}\right) \mathrm{Im}(n_{\mathrm{eff}}),\ \mathrm{cm}^{-1} \tag{6}$$

where, c indicates the speed of light in vacuum and $\mathrm{Im}(n_{\mathrm{eff}})$ represents the imaginary part of the complex refractive index.

Figs. 13 and 14 indicates the characteristics of confinement loss with respect to frequency at optimum core air hole dimensions of PCF-I and PCF-II respectively. In both the cases, it can be seen that confinement loss decreases as the frequency increases. This is because, light confines more strongly in the porous core region as frequency increase. At optimum frequency and other design conditions the experienced confinement loss for both the PCF is negligible as compared to the

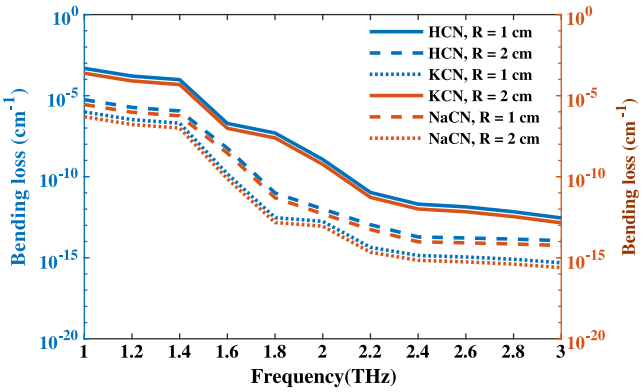

Fig. 15. Bending loss of PCF-I with respect to frequency at optimum value of $(d_{c_1}) = 46.6$ μm and $d = 6$ μm.

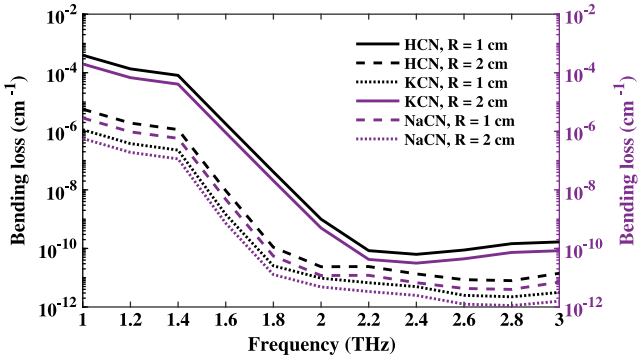

Fig. 16. Bending loss of PCF-II with respect to frequency at optimum value of $W = 24.75$ μm and $d = 6$ μm.

obtained EML. Negligible confinement loss is suitable for long length sensing operation of terahertz sensor.

Bending loss is also an important loss mechanism that occurs when the fiber is bent that can be calculated by the following equation [23,24],

$$n_{\mathrm{eq}}(x, y) = n(x, y)\ \left(1 + \left(\frac{x}{R}\right)\right),\ \mathrm{cm}^{-1} \tag{7}$$

where, $n_{\mathrm{eq}}(x, y)$ is the modified refractive index profile after bent, $n(x, y)$ is actual refractive index of the used material, x represents the distance from the center of the PCF to the bending point, and R represents the bending radius.

Figs. 15 and 16 represents the bending loss of the proposed sensor. It can be observed that bending loss decreases with increased R. Due to the bending of the PCF, the fundamental mode shifts towards the cladding and thus bending loss increases. Note that higher bending means reduced bending radius R. After getting the modified refractive index profile of the PCF the bending loss can be calculated using the same formula as mention in Eq. (6). Upon observing Figs. 15 and 16, it can be seen that the bending loss is negligible as compared to the obtained EML. Negligible bending loss is suitable for sensing application where the fiber need to be bent.

Birefringence of a fiber can be defined as the index difference between the polarization modes that can be calculated by the following equation,

$$B = |n_x - n_y| \tag{8}$$

here, B represents birefringence, n_x and n_y are the effective refractive index of the polarization modes.

To improve the sensing performance, polarization preserving property of a fiber is important. Asymmetrical structure both in core and

Table 1
Comparison of characteristics of PCF-I and PCF-II considering HCN as the analyte.

Sensor type	Optimum frequency	Relative sensitivity	EML (cm^{-1})	Con. loss (cm^{-1})	Bend. loss (cm^{-1}) (R = 1 cm)	B
PCF-I	2.0 THz	85.8%	0.023	1.62×10^{-9}	1.14×10^{-9}	0.009
PCF-II	1.8 THz	77.5%	0.031	5.15×10^{-8}	4.09×10^{-8}	0.049

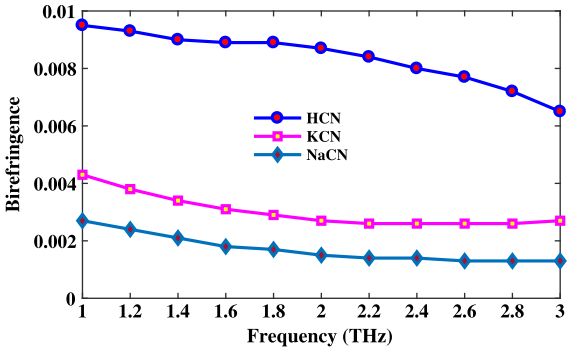

Fig. 17. Birefringence of PCF-I with respect to frequency at optimum design conditions.

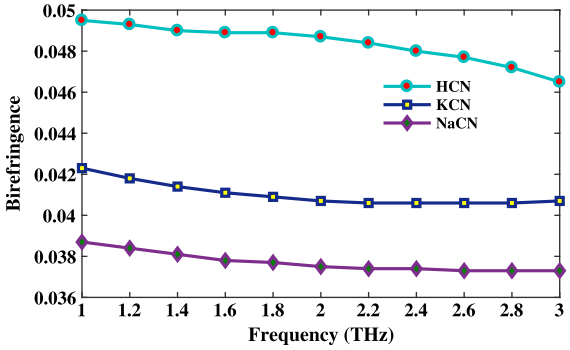

Fig. 18. Birefringence of PCF-II with respect to frequency at optimum design conditions.

cladding help to improve the birefringence property of a PCF. It can be calculated by the index difference of the orthogonal polarization modes. Figs. 17 and 18 shows the birefringence of PCF-I and PCF-II respectively. Figs. 17 and 18 indicates that HCN experiences higher birefringence than KCN and NaCN. This is because HCN have low refractive index than KCN and NaCN that introduces larger index difference between the polarization modes. Note that, due to larger asymmetry both in core and cladding, PCF-II experiences higher birefringence than PCF-I.

The sensor architecture will be a combination of few optical and electrical elements where the proposed fiber will work as an active sensing element. The analyte in the micro-structured air holes will be filled either by slowly feeding the channel by hepodermic needle or the analyte filling can be done by depositing a layer in one end of the fiber so that it can block analyte entering into the cladding. Moreover, using the birefringence effect the proposed sensor will use the absorption of analytes as a sensing mechanism [22].

A comparison of obtained characteristics of both PCF-I and PCF-II is shown in Table 1. It clearly indicates that, in terms of sensitivity PCF-I shows improved performance whereas in terms of birefringence PCF-II shows better performance. As birefringence is an important property for improving the sensing performance thus PCF-II has improved performance over PCF-I.

4. Fabrication possibilities of the proposed PCF based terahertz sensor

We can see from the proposed PCFs that it consists of circular, rectangular and elliptical shaped air holes. Thus in order to fabricate the proposed PCFs it is necessary to have fabrication methods that can fabricate all the three air hole structure. Note that, there are a number of well developed fabrication technologies nowadays such as capillary stacking, drilling, sol–gel, extrusion and 3D printing that have potential to fabricate PCF. Among them the capillary stacking and sol–gel techniques are suitable to fabricate circular shaped air holes [24]. The extrusion and 3D printing technology are able to fabricate different complex shaped asymmetrical air hole structure including rectangular, square, and elliptical. The extrusion technique allows fabrication of different types of air hole structure including the elliptical shaped air holes [19,20,25–27]. Therefore, with recent advances in prevailing fabrication techniques, the proposed PCFs can be made.

5. Conclusion

We have presented the characteristics comparison of two different types of PCF based terahertz sensor. Using Zeonex as the background material we investigated the sensing performance of both the sensors in terahertz band. Simulation results indicate that, PCF-I shows higher relative sensitivity than PCF-II. However, as polarization preserving characteristics is important in improving the sensing performance, PCF-II is considered to be improved over PCF-I as PCF-II contains greater asymmetry than PCF-I. Both the PCFs are realizable using existing fabrication technologies. Thus, considering the sensing performances and simplicity in sensor architectures it can be said that the proposed sensors will open a new window for further research on terahertz sensing. Moreover, we believe that, with suitable commercialization the proposed sensors will be a suitable candidate for harmful cyanide detection at terahertz frequency band.

Acknowledgements

Funding from the Australian Research Council (DP170104984) is gratefully acknowledged.

References

[1] R. Jackson, B.A. Logue, A review of rapid and field-portable analytical techniques for the diagnosis of cyanide exposure, Anal. Chim. Acta 960 (2017) 18–39.
[2] I. Petrikovics, M. Budai, K. Kovacs, D.E. Thompson, Past, present and future of cyanide antagonism research: From the early remedies to the current therapies, World J. Methodol. 5 (2) (2015) 88–100.
[3] Z. Xu, X. Chen, H.N. Kim, J. Yoon, Sensors for the optical detection of cyanide ion, Chem. Soc. Rev. 39 (1) (2010) 127–137.
[4] E. Jaszczak, M. Ruman, S. Narkowicz, J. Namienik, Polkowska, Development of an analytical protocol for determination of cyanide in human biological samples based on application of ion chromatography with pulsed amperometric detection, J. Anal. Methods Chem. 2017 (2017) 7157953.
[5] Y.G. Timofeyenko, J.J. Rosentreter, S. Mayo, Piezoelectric quartz crystal microbalance sensor for trace aqueous cyanide ion determination, Anal. Chem. 79 (1) (2007) 251–255.
[6] T. Suzuki, A. Hiolki, M. Kurahashi, A convenient colorimetric and ratiometric fluorescent probe for detection of cyanide based on BODIPY derivative in aqueous media, Anal. Chem. Res. 12 (1) (2017) 34–39.
[7] J. Sánchez, M. del Valle, Determination of anionic surfactants employing potentiometric sensors — a review, Crit. Rev. Anal. Chem. 35 (1) (2007) 15–29.
[8] J. Wu, L. Wang, Q. Wang, L. Zou, B. Ye, The novel voltammetric method for determination of hesperetin based on a sensitive electrochemical sensor, Talanta 150 (2016) 61–70.

[9] L. Liu, X. Wang, J. Yang, Y. Bai, Colorimetric sensing of selenocystine using gold nanoparticles, Anal. Biochem. 535 (2017) 19–24.
[10] T.M. Monro, W. Belardi, K. Furusawa, J.C. Baggett, N.G.R. Broderick, D.J. Richardson, Sensing with microstructured optical fibres, Meas. Sci. Technol. 12 (7) (2001) 854.
[11] C.M.B. Cordeiro, M.A.R. Franco, G. Chesini, E.C.S. Barretto, R. Lwin, C.H.B. Cruz, M.C.J. Large, Microstructured-core optical fibre for evanescent sensing applications, Opt. Express 14 (26) (2006) 13056–13066.
[12] X.-d. Wang, O.S. Wolfbeis, Fiber-optic chemical sensors and biosensors, Anal. Chem. 88 (1) (2016) 203–227.
[13] V. Kaur, S. Singh, Extremely sensitive multiple sensing ring PCF sensor for lower indexed chemical detection, Sens. Bio-Sens. Res. 15 (2017) 12–16.
[14] H. Ademgil, Highly sensitive octagonal photonic crystal fiber based sensor, Optik 125 (20) (2014) 6274–6278.
[15] H. Ademgil, S. Haxha, Highly PCF based sensor with high sensitivity, high birefringence and low confinement losses for liquid analyte sensing applications, Sensors 15 (12) (2015) 31833–31842.
[16] M.S. Islam, J. Sultana, K. Ahmed, A. Dinovitser, M.R. Islam, B.W.-H. Ng, D. Abbott, A novel approach for spectroscopic chemical identification using photonic crystal fiber in the terahertz regime, IEEE Sens. J. 18 (2) (2018) 575–582.
[17] M.S. Islam, J. Sultana, K. Ahmed, A. Dinovitser, M. Faisal, M.R. Islam, B.W.-H. Ng, D. Abbott, A novel Zeonex based photonic sensor for alcohol detection in beverages, in: IEEE International Conference on Telecommunications and Photonics, ICTP, Dhaka, Bangladesh, 2017, pp. 114–118. http://dx.doi.org/10.1109/ICTP.2017.8285905.
[18] G. Woyessa, A. Fasano, C. Markos, A. Stefani, H.K. Rasmussen, O. Bang, Zeonex microstructured polymer optical fiber: fabrication friendly fibers for high temperature and humidity insensitive Bragg grating sensing, Opt. Mater. Express 7 (1) (2017) 286–295.
[19] H. Ebendorff-Heidepriem, J. Schuppich, A. Dowler, L. Lima-Marques, T. Monro, 3D-printed extrusion dies: A versatile approach to optical material processing, Opt. Mater. Express 4 (8) (2014) 1494–1504.
[20] S. Atakaramians, S. Afshar, H. Ebendorff-Heidepriem, M. Nagel, B.M. Fischer, D. Abbott, T.M. Monro, THz porous fibers: design, fabrication and experimental characterization, Opt. Express 17 (16) (2009) 14053–14062.
[21] S. Rana, A.S. Rakin, H. Subbaraman, R. Leonhardt, D. Abbott, Low loss and low dispersion fiber for transmission applications in the terahertz regime, IEEE Photon. Technol. Lett. 29 (10) (2017) 830–833.
[22] M.S. Islam, J. Sultana, A.A. Rifat, A. Dinovitser, B.W.-H. Ng, D. Abbott, Terahertz sensing in a hollow core photonic crystal fiber, IEEE Sens. J. (2018). http://dx.doi.org/10.1109/JSEN.2018.2819165.
[23] S. Ali, N. Ahmed, S. Aljunid, B. Ahmad, Hybrid porous core low loss dispersion flattened fiber for THz propagation, Photon. Nanostruct.: Fundam. Appl. 22 (2016) 18–23.
[24] R. Islam, G.K.M. Hasanuzzaman, Md.S. Habib, S. Rana, M.A.G. Khan, Low-loss rotated porous core hexagonal single-mode fiber in THz regime, Opt. Fiber Technol. 24 (2015) 38–43.
[25] N.A. Issa, M.A.V. Eijkelenborg, M. Fellew, F. Cox, G. Henry, M.C.J. Large, Fabrication and study of microstructured optical fibers with elliptical holes, Opt. Lett. 29 (12) (2004) 1336–1338.
[26] F. Liu, H. Gao, Q. Xu, Y. Zhang, Fabrication and characteristics of elliptical-holes and near elliptical core hexangular lattice photonic crystal fibers based on polymer, Adv. Mater. Res. 279 (2011) 151–156.
[27] S. Atakaramians, Terahertz Waveguides: A Study of Microwires and Porous Fibre (Ph.D. thesis), The University of Adelaide, 2011, pp. 146–156, Chapter 5. Available: https://digital.library.adelaide.edu.au/dspace/handle/2440/69317.